Modeling the Electron Transfer Chain in an Artificial Photosynthetic Machine

Umberto Raucci, Marika Savarese, Carlo Adamo, Ilaria Ciofini, Nadia Rega

Toward the Theoretical Design of Artificial Photosynthetic Machines

Umberto Raucci[1], Marika Savarese[1], Carlo Adamo[2,3], Ilaria Ciofini[2], and Nadia Rega[1,4,*]

[1]*Dipartimento di Scienze Chimiche, Università di Napoli Federico II, Complesso Universitario di M.S. Angelo, via Cintia, I-80126 Napoli, Italy.*
[2]*Chimie ParisTech, PSL University, CNRS, Institute of Chemistry for Life and Health Sciences, Theoretical Chemistry and Modelling, 75005 Paris, France.*
[3]*Institut Universitaire de France, 103 Boulevard Saint Michel, F-75005 Paris, France.*
[4]*CRIB, Centro Interdipartimentale di Ricerca sui Biomateriali P.zzale Tecchio, I-80125 Napoli, Italy.*

**correspondence nadia.rega@unina.it*

Abstract:

The development of efficient artificial leaves relies on the subtle combination of molecular assemblies able to absorb sunlight, converting light energy into electrochemical potential energy and finally transducing it into chemical accessible energy. The electronical design of these charge transfer molecular machines is crucial to build a complex supramolecular architecture for the light energy conversion. Here, we present an *ab initio* simulation of the whole decay pathways of a recently proposed artificial molecular reaction center. A complete structural and energetic characterization has been carried out with methods based on density functional theory, its time dependent version and broken symmetry approach. On the basis of our findings we provide a relevant revision of the pathway only indirectly postulated from an experimental point of view, along with unprecedented and significant insights on the electronic and nuclear structure of intramolecular charge separated states, which are fundamental for the application of this molecular assembly in photoelectrochemical cells. Importantly, we unravel the molecular driving forces of the various charge transfer steps, in particular those leading to the proton coupled electron transfer final product, highlighting key elements for the future design strategies of such molecular assays.

Main Text:

Conversion of light into electric or chemical energy is undoubtedly a very attractive solution for the global energy problem.[1-10] Analogously, storage of solar energy into chemical fuels through the development of efficient photoelectrochemical cells (PECs)[11-13] opens the route for new and environmentally friendly energy sources. Nevertheless, the development of these devices is not straightforward since several entangled processes have to be finely combined and controlled (i.e light harvesting, charge separation, electron transfer). The best inspiration for the design of such devices is definitely provided by Nature that developed an extremely efficient molecular machine -the photosystem II (PSII)- able to convert sunlight into chemically accessible energy.[8-10, 14]

PSII uses solar photons to drive the oxidation of water to dioxygen in an amazing way, combining different specialized molecular units (e.g. chlorophyll complex P680, oxygen evolving center, redox active tyrosine-histidine pair).[14-16] Therefore, this system is an optimum starting point for the construction of artificial photosynthetic machines. In this perspective, Moore and co-workers proposed a molecular triad (hereafter named BiPhOH-PF_{10}-TCNP and depicted in **Figure 1**) functionally mimicking the highly efficient initial photo-induced charge separated state in PSII.[17] This system is composed by : i) a functionalized porphyrin moiety (PF_{10}) acting as primary electron donor and mimicking the chlorophyll P680 exciton trap of PSII; ii) a tetracyanoporphyrin (TCNP) ring that acts as electron acceptor simulating the pheophytin moiety; and iii) a benzimidazole-phenol group (BiPhOH) that models the tyrosine hystidine pair of PSII. This pair is involved in a Proton Coupled Electron Transfer (PCET) reaction during the photosynthetic cycle. Moore and co-workers provided a detailed

spectroscopic and electrochemical characterization of this molecular triad leading to the complex decay pathways reported in the inset of **Figure 2**.[17] Based on experimental data, their hypothesis is that the initial excitation of the PF_{10} group is followed by singlet energy transfer to the TCNP moiety, whose excited state can relax by a photoinduced electron transfer (PET) toward a charge separated state giving rise to a Bi-PhOH-$PF_{10}^{+\cdot}$-$TCNP^{-\cdot}$ species. They proposed that this species rapidly undergoes a PCET reaction in which an electron is transferred from the phenol to the $PF_{10}^{+\cdot}$ group, while the phenolic proton is transferred towards the benzimidazole group providing the final species, postulated to be the BiH^{+}-$PhO^{\cdot}$-PF_{10}-$TCNP^{-\cdot}$ molecule. Since time resolved spectra suggest that this charge separated state has a long lifetime and an high redox potential, this triad becomes particularly attractive for the development of new PEC devices.[17]

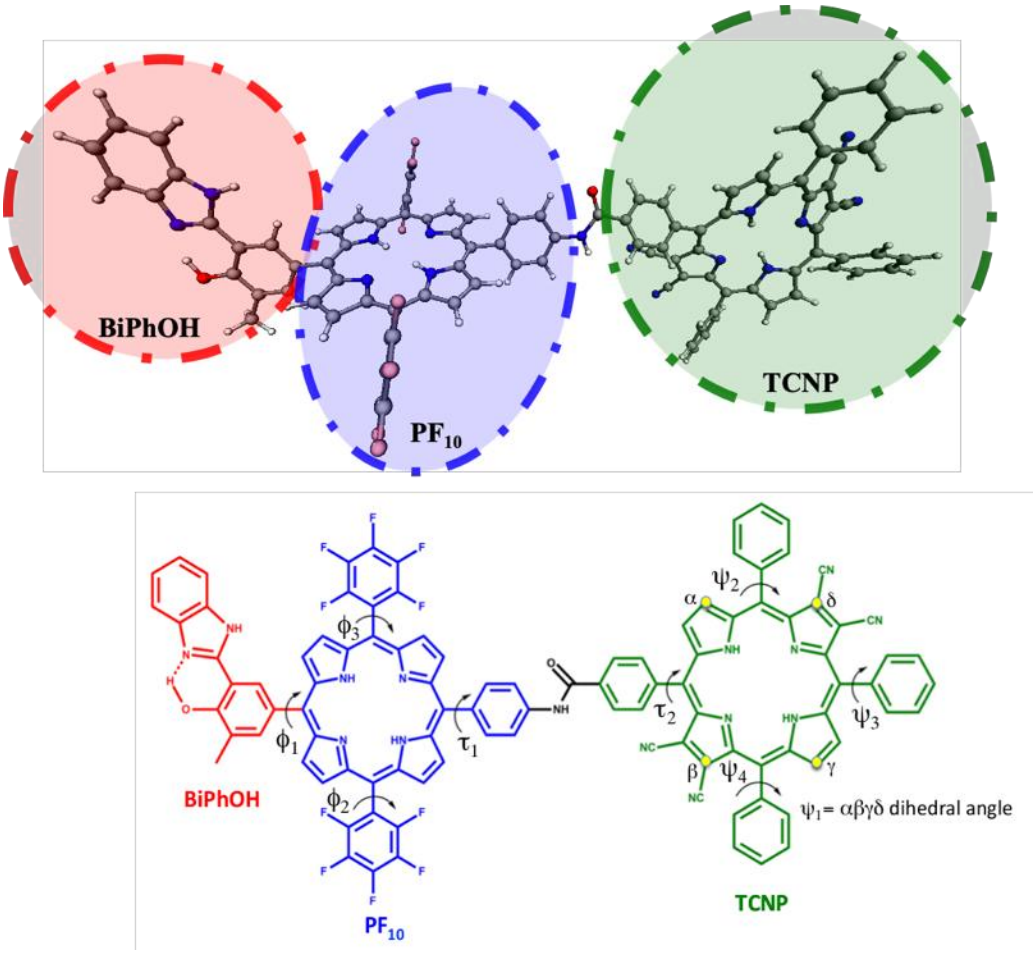

Figure 1. Molecular structure of triad BiPhOH-PF_{10}-TCNP composed of three covalently linked subunits: BiPhOH, PF_{10} and TCNP. Labelling of critical dihedral angles is also provided. The dihedral angle Ψ_1 is that defined by the α, β, γ, δ atoms.

Nevertheless, for the time being, the nature and the relative energies of all the electronic states involved in this complex mechanism have been only experimentally and indirectly estimated by combining redox measurements with absorption and emission data of isolated form of the three molecular fragments composing the triad. At the present, no clear direct evidence for the formation of the final PCET product have been obtained from experiments. Indeed, in a recent publication[4] Moore and co-worker stated that "indirect evidence for PCET comes from reduction potentials of model compounds [18] which indicate that PF_{10} would not generate sufficient driving force for the formation of the Bi-$PhOH^{\bullet +}$-PF_{10}-$TCNP^{- \bullet}$ and thus implies the formation of the BiH^{+}-$PhO^{\bullet}$-PF_{10}-$TCNP^{- \bullet}$ state." [4]

In order to tune and control the properties of such a triad as well as to help in the design on new systems a more detailed knowledge of the electronic structure of all the intermediate states involved in the excited state evolution is mandatory. Here, for the first time, we provide a complete theoretical structural and energetic characterization of all the crucial species involved in the decay pathway (Bi-PhOH-$PF_{10}^{+ \bullet}$-$TCNP^{- \bullet}$, Bi-$PhOH^{\bullet +}$-PF_{10}-$TCNP^{- \bullet}$ and BiH^{+}-$PhO^{\bullet}$-PF_{10}-$TCNP^{- \bullet}$). By studying the complete triad we show how the final PCET product, BiH^{+}-$PhO^{\bullet}$-PF_{10}-$TCNP^{- \bullet}$, is energetically more stable than the Bi-$PhOH^{\bullet +}$-PF_{10}-$TCNP^{- \bullet}$ side adduct, highlighting the principal structural differences between them. Furthermore, we investigate the proton coupled electron transfer reaction reconstructing the reaction path and individuating the structural motifs driving it. Describing the driving force of the various charge transfer steps is one of our principal aims, especially to support the future design strategies of such molecular devices.

The theoretical simulation of the experimentally proposed decay pathways it's far from being straightforward due to the necessity of accurately simulating the excited state evolution of a large system in presence of a medium –the solvent- with can play an important role in the stabilization of the different states.

Density Functional Theory (DFT)[19] and its time dependent counterpart (TD-DFT) level[20-21] offer valuable tools for the description of excited states processes in condensed phase,[22-25] although this choice makes the accurate simulation of excited states with a net intramolecular charge transfer character far to be trivial.[26-27] For this reason, we complemented the TD-DFT description of such states resorting on the broken symmetry approach (BS) originally developed by Noodleman and co-workers [28-31] to describe magnetic coupling[32] and thus open shell singlet states using a single determinant approach. This kind of approach enables the setup of computationally stable protocols for the description of excited state dealing with charge transfer processes, which might be of interest in the design of new synthetic models for photoelectrochemical devices.

To simplify the following discussion each excited state of the triad will be labelled as S^X_n. The X superscript identifies the diabatic composition of the excited state based on the molecular moiety mostly involved in the excitation (e.g. X can be TCNP or PF_{10}) while the subscript n specifies the adiabatic electronic state number according to its energy. S indicates that each excited state computed is a singlet. The computational details are provided in the Supplemental Information (SI).

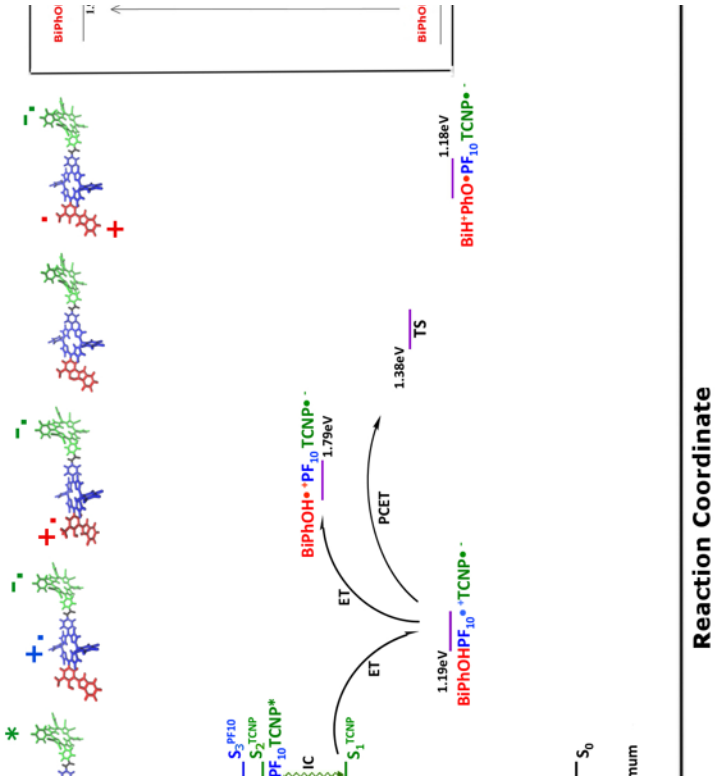

Figure 2. Simulated decay pathway for BiPhOH-PF_{10}-TCNP. Excitation, Internal conversion (IC), Energy Transfer (EnT), Electron Transfer (ET) and Proton Coupled Electron Transfer (PCET) steps are represented. Energy levels have been computed at TD-DFT and Broken Symmetry level of theory. The vertically computed excited states are reported in the Franck Condon region, and S_2 energy minimum. For comparison, in the inset it is reported the experimentally proposed energy level diagram of decay pathways for triad according to ref. [17].

Initially the triad is excited from its ground electronic state (S_0). The two subunits PF_{10} and TCNP of BiPhOH-PF_{10}-TCNP are almost perpendicular in S_0, while the BiPhOH and PF_{10} rings are twisted by roughly 67° (Φ_1=-67°, see **Figure 1** for the labelling and **Table 1** for the values of the other principal dihedral angles) suggesting a certain electronic coupling among them. The PF_{10} moiety is highly symmetric with the pentafluorephenyl groups similarly oriented with respect to the plane of the porphyrin ring. The TCNP unit assumes a non-planar structure due to steric interactions between the cyano and phenyl groups, respectively in the beta and meso positions of the tetrapyrrolic ring. Steric interactions also lead to an orientation for the phenyl groups far from the perpendicular one (see Ψ_2, Ψ_3, and Ψ_4 dihedral angles in **Table 1** and **Figure 1**). The experimental absorption spectrum for the triad in benzonitrile shows two intense broad bands in the Soret regions centred at 2.76 and 2.92 eV, respectively. TD-DFT results show two

intense electronic transitions at 3.00 eV (oscillator strength f=2.966, state S_6^{TCNP}) and 3.16 eV (f=2.157, state S_7^{PF10}) localized respectively on the TCNP and on the PF_{10} groups. Starting from the absorption event, the simulated pathway can be followed by inspecting **Figure 2**.

Electronic state	Φ_1	Φ_2	Φ_3	τ_1	τ_2	ψ_1	ψ_2	ψ_3	ψ_4
S_0	-67.14	-108.88	108.38	-113.75	-113.45	-14.55	-66.54	-114.48	-67.64
S_2^{TCNP}	-68.13	-109.72	109.47	-113.84	-117.84	-18.16	-62.86	-117.68	-64.13
S_1^{TCNP}	-68.15	-109.58	109.02	-113.38	-127.11	-25.03	-52.79	-127.32	-53.64
$BiPhOH\text{-}PF_{10}^{+\cdot}\text{-}TCNP^{\cdot-}$	-54.28	-111.88	107.24	-121.68	-117.79	-17.61	-62.92	-117.88	-64.33
$BiH^{+}PhO^{\cdot}\text{-}PF_{10}\text{-}TCNP^{\cdot-}$	-49.54	-109.92	105.38	-115.88	-118.63	-17.77	-63.03	-117.94	-64.09
$BiPhOH^{+\cdot}\text{-}PF_{10}\text{-}TCNP^{\cdot-}$	-92.11	-109.33	108.68	-115.81	-117.99	-17.54	-63.49	-117.49	-64.21

Table 1. Characteristic dihedral angles (in degree, refer to **Figure 1** for labels) computed for the triad in the relevant electronic states. All parameters are computed on the relative minimum energy structure.

After the excitation to the state S_7^{PF10} a fast internal conversion to a state still localized on PF_{10} but at lower energy (state S_2^{PF10}) can take place (see **Figure 2**). This is in line with the photochemistry of porphyrin molecules that, following the absorption to higher excited electronic states, give rapid internal conversion to S_1, from where emission is observed.[33] The S_2^{PF10} state has been vertically computed at 2.11 eV (f=0.017) on the S_0 minimum energy structure and it is characterized by the transition between frontier molecular orbitals reported in **Figure S1**. Another excited state (S_3^{TCNP}) can be found close in energy to S_2^{PF10}, and it is calculated at 2.13 eV (f=0.103) in the S_2^{PF10} Franck Condon region. This state is characterized by an electronic excitation completely localized on the TCNP unit.

S_2^{PF10} and S_3^{TCNP} are the main actors involved in the excitation transfer from the PF_{10} to the TCNP moieties. Starting from the Franck Condon region, a change in the S_2 locally excited character from PF_{10} to TCNP can easily occur by coupling to the S_3 potential energy surface. In **Figure S2** we report energy profiles along a linear synchronous path coordinate linking the S_2^{PF10} and S_2^{TCNP} energy minimum structures, clearly showing the possible change in the S_2 character from PF_{10} to TCNP by a non-adiabatic coupling with the S_3 potential surface.

Thus, the global energy minimum in the S_2 adiabatic state involves an electronic excitation completely localized on the TCNP unit (S_2^{TCNP}). This step corresponds to the experimentally hypothesized energy transfer from PF_{10} to TCNP in the triad (first step in the **Figure 2** inset).

The TCNP ring distortion is one the main degree of freedom involved in the S_2^{PF10} toward S_2^{TCNP} path. Indeed, starting from the Franck Condon region, the Ψ_1 dihedral angle changes of about 4 degrees when passing to the S_2^{TCNP} excited state energy minimum.

The fluorescence from the TCNP is experimentally observed at 1.72 eV and it is computed at 2.02 eV (f=0.409) in the S_2^{TCNP} excited state energy minimum. From an experimental point of view, it has been hypothesized that this state corresponds to the reactant for the first ET process (see inset in **Figure 2**). Nevertheless, from our calculations it was no possible to individuate a CT character from the PF_{10} to the TCNP unit in structures close to the S_2^{TCNP} energy minimum, which would have been a reasonable indication of the possible ET process. Indeed, in this structure another electronic excited state (S_1^{TCNP}) with energy of 1.63 eV (f=0.473) has been calculated, characterized by an electronic excitation still completely localized on the TCNP group (**Figure S1** for the MOs involved in the transition). The main difference between the S_2^{TCNP} and S_1^{TCNP} states is a significant change of both the electronic and nuclear arrangements during the S_1^{TCNP} relaxation. As matter of fact, the charge transfer character of the S_1^{TCNP} excitation drastically increases when going from the S_2^{TCNP} to the S_1^{TCNP} minimum energy structure: while at the S_2^{TCNP} minimum the MOs involved in the S_1^{TCNP} transition are completely localized on the TCNP moiety, the character of charge transfer from the PF_{10} to the TCNP unit increases at the S_1^{TCNP} minimum energy structure (see **Figure S3** for the MOs involved in the electronic excitation). Considering that the energy difference (0.39 eV) between S_1^{TCNP} and

S_2^{TCNP} corresponds to about 3100 cm^{-1}, we propose an internal conversion occurring between the S_2^{TCNP} and S_1^{TCNP} states, and assume the S_1^{TCNP} state as the electron transfer reactant (**Figure 2**).

The distortion of the TCNP tetrapyrrolic ring is the main degree of freedom involved during the structural relaxation of S_1^{TCNP} and it promotes the charge transfer from the PF_{10} to the TCNP unit (see **Table 1**). Indeed, the Ψ_1 dihedral angle, describing the distortion of the porphyrin ring, changes from -18° to -25° during this relaxation, driving the variation in the nature of the MOs involved in the S_1^{TCNP} electronic transition. This deformation increases the steric repulsions between the cyano and phenyl groups that, in turn, assume a more planar orientation with respect to the porphyrin ring. The TCNP deformation is, thus, a key structural motif for the charge transfer event. Interestingly, this change in the nature of the excited S_1^{TCNP} state was observed only for calculations performed in benzonitrile solution, while it was not reproduced in analogue S_1^{TCNP} optimization in cyclohexane. In this case, the excitation remains localized on the TCNP moiety. This clearly indicates that only polar solvents with high dielectric constant are able to stabilize the electron transfer product and it is in fair agreement with the experimental evidences indicating that a high quantum yield for the PET reaction is observed only in polar medium (benzonitrile). The energy of the relaxed S_1^{TCNP} state is computed at 1.40 eV (f=0.565). Within the TD-DFT framework this is the best picture of the electron transfer product. In order to describe the evolution of this charge separated state in the ET product, the BS approach was applied. An open shell BS singlet state characterized by a spin density localized on both the PF_{10} and the TCNP groups was computed. The spin density plot and the Mulliken spin density (MSD) integrated for fragments are reported for this structure in **Figure 3a,** with the fragment definition provided in **Figure S4**.

Looking at the fragments MSD it's clear that the BS calculated singlet state represents the PET product, namely the Bi-PhOH-$PF_{10}^{+\cdot}$-TCNP$^{-\cdot}$ adduct. Indeed, two unpaired electrons with opposite spin are localized on the PF_{10} and TCNP moieties, respectively, with negligible contribution on the BiPhOH group. The Mulliken charge analysis for fragments reveals a net positive charge of +1.10 on the PF_{10} unit and a net negative charge of -0.93 on the TCNP fragment. This configuration is that expected following an electron transfer from the PF_{10} to the TCNP group. The Bi-PhOH-$PF_{10}^{+\cdot}$-TCNP$^{-\cdot}$ species, on turn, represents the reactant for the next PCET step.

In order to characterize the PCET reaction, we chose the phenol oxygen– hydrogen ($O_{Ph}H$) distance as degree of freedom representative of the proton transfer coordinate. We obtained an energy profile by a relaxed scan along this coordinate at TD-DFT level. The S_1^{TCNP} electronic structure showed only a negligible variation along this coordinate, that means no ET accompanied the PT event.

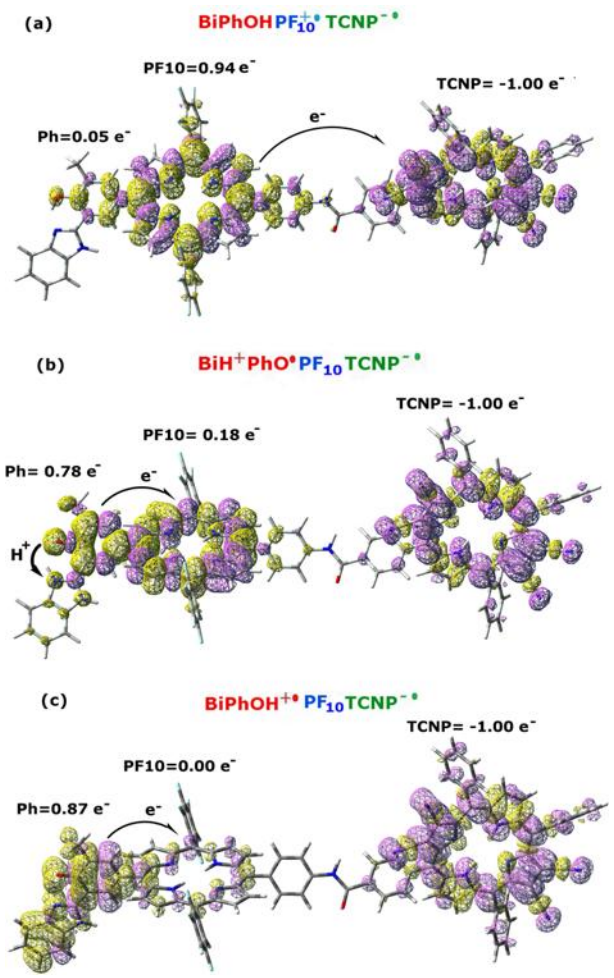

Figure 3. (a) Spin density plot for the electron transfer product (Bi-PhOH-$PF_{10}^{+\cdot}$-$TCNP^{-\cdot}$) in the broken symmetry approximation. **(b)** Spin density for the proton coupled electron transfer product (BiH^{+}-$PhO^{\cdot}$-PF_{10}-$TCNP^{-\cdot}$). **(c)** Spin density plot for the electron transfer product (Bi-$PhOH^{\cdot +}$-PF_{10}-$TCNP^{-\cdot}$). Integration for fragments of the Mulliken spin density is also reported.

On the other hand, a BS solution was obtained on the PT product, corresponding to the BiH^{+}-$PhO^{\cdot}$-PF_{10}-$TCNP^{-\cdot}$ PCET adduct. In **Figure 3b** we showed the spin density plot and the MSD integrated for fragments of this species. This latter analysis shows the electronic holes localized on both the TCNP (-1.0e^{-}) and phenol (0.78e^{-}) units. The $O_{Ph}H$ distance is 1.863 Å in this structure, while the imidazole nitrogen – hydrogen (N_{Im}-H) distance is 1.023 Å.

We also observed a small spin polarization on the PF_{10} moiety. This is principally due to the strong electronic coupling between the BiPhOH and PF_{10}. The transition state (TS) for the PCET

step has been also computed (the spin density plot is reported in **Figure S5**), with an imaginary frequency at -1169cm^{-1} (the displacement vectors for the imaginary frequency at the transition state are reported in **Figure S6**). The $O_{Ph}H$ and N_{Im}-H distance are respectively of 1.272 and 1.205 Å at the transition state. The integration of the intrinsic reaction coordinate has been also carried out in order to follow the variation of the spin density along the reaction path (**Figure 4a**). **Figure 4a** shows that starting from the Bi-PhOH-$PF_{10}^{+\cdot}$-TCNP$^{-\cdot}$ species, an electron is transferred from the phenol toward the PF_{10} group saturating its electronic hole when the proton is bounded to the imidazole nitrogen. The spin density on the TCNP fragment is constant, revealing the formation of the BiH^{+}-$PhO^{\cdot}$-PF_{10}-$TCNP^{-\cdot}$ species. In spite of a barrier of 4.44 kcal/mol, the PCET product is slightly favoured of about 0.16 kcal/mol.

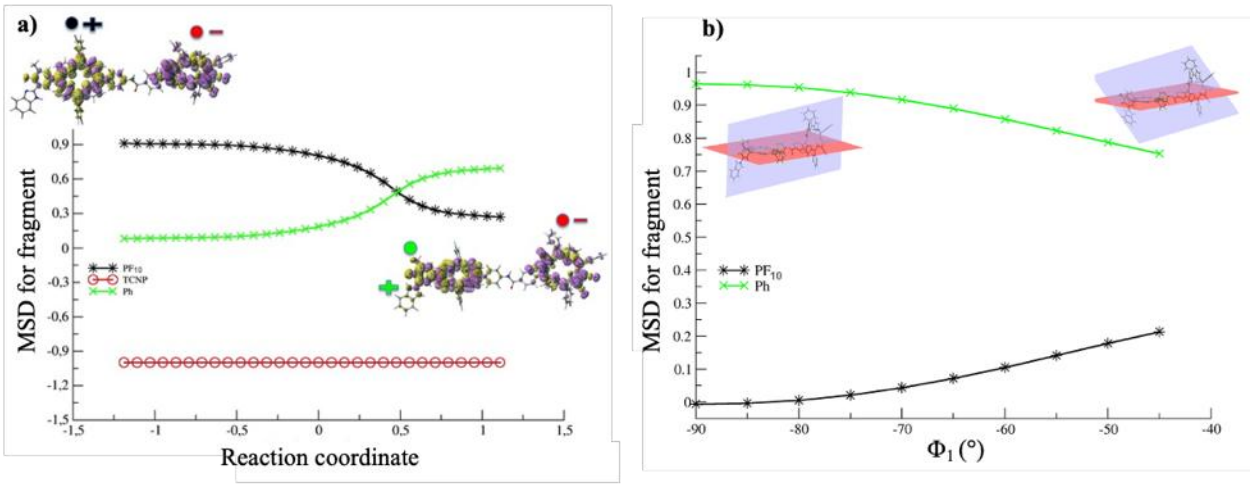

Figure 4. (a) Mulliken spin density (MSD) integrated for fragment along the IRC for the PCET reaction. **(b)** Mulliken spin density integrated for fragment along the variation of the Φ_1 dihedral angle on the BiH^{+}-$PhO^{\cdot}$-PF_{10}-$TCNP^{-\cdot}$ state.

From a mechanistic point of view, the Φ_1 dihedral angle is the degree of freedom principally involved in the PCET reaction (see **Table 1**). This angle defines the relative orientation between the BiPhOH and the PF_{10} units varying of about 5 degrees during the reaction. Φ_1 is an important

parameter controlling the electronic coupling between the two units, thus modulating the electron transfer among them. To further analyse this point, the variation of the MSD on the PF_{10} and Ph fragments with respect to the Φ_1 dihedral angle is reported in **Figure 4b**. This plot has been obtained scanning the Φ_1 dihedral angle from -45° to -90° on the broken symmetry BiH^{+}-$PhO^{\cdot}$-PF_{10}-$TCNP^{-\cdot}$ state. When the two rings are almost perpendicular (Φ_1 = -90°) the spin density on the PF_{10} fragment is zero and that on Ph is about one. Varying the Φ_1 angle the spin density on the PF_{10} moiety gradually increases, reaching its maximum value (about 0.2) when the two rings become more planar. At the same time the spin density on the Ph fragment decreases reaching at least the value of about 0.8. This internal mode is crucial to drive the PCET event, and it has to be considered as a critical motif for the future design of these charge transfer molecular machines.

We also computed the alternative BS solution corresponding to the transfer of an electron from the Ph group towards the PF_{10} one, with no PT between phenol and benzimidazole groups, namely the Bi-$PhOH^{\cdot +}$-PF_{10}-$TCNP^{-\cdot}$ species, (**Figure 3c**).

This state is found to lie 0.60 eV (13.89 kcal/mol) higher in energy with respect to the Bi-PhOH-$PF_{10}^{+\cdot}$-$TCNP^{-\cdot}$ one (**Figure 2**). Its formation is, thus, energetically unfavourable. Once again Bi-$PhOH^{\cdot +}$-PF_{10}-$TCNP^{-\cdot}$ and Bi-PhOH-$PF_{10}^{+\cdot}$-$TCNP^{-\cdot}$ differ principally for the mutual orientation of the BiPh and PF_{10} moiety, namely for the Φ_1 dihedral angle (**Table 1**). Indeed, this degree of freedom changes of about 40° between the two structures, with the Bi-$PhOH^{\cdot +}$-PF_{10}-$TCNP^{-\cdot}$ species favoured by the perpendicular arrangement between the Ph and PF_{10} rings.

In conclusion, the complete excited state cascade of the triad BiPhOH-PF_{10}-TCNP has been simulated within the TD-DFT and BS frameworks. This combined approach allowed to describe the complexity of the structural and electronic evolution of the charge transfer steps following

the electronic excitation of the triad. Furthermore, the internal degrees of freedom involved during the various steps have been successfully analysed. We individuate the dihedral angles involved in the modulation of the electronic coupling between the BiPhOH and PF_{10} moieties as crucial parameters for the formation of the various charge transfer species.

The combination of TD-DFT and broken symmetry approaches paves the way to disentangle the complex electronic structure of PSII mimics and for the successful design of charge transfer molecular machines suitable for artificial photosynthesis.

References:

1. Grätzel, M. Recent Advances in Sensitized Mesoscopic Solar Cells. *Acc. Chem. Res.* **2009,** *42* (11), 1788-1798.
2. Berardi, S.; Drouet, S.; Francàs, L.; Gimbert-Suriñach, C.; Guttentag, M.; Richmond, C.; Stoll, T.; Llobet, A. Molecular artificial photosynthesis. *Chem. Soc. Rev.* **2014,** *43* (22), 7501-7519.
3. Gust, D.; Moore, T. A.; Moore, A. L. Realizing artificial photosynthesis. *Faraday Discuss.* **2012,** *155* (0), 9-26.
4. Llansola-Portoles, M. J.; Palacios, R. E.; Gust, D.; Moore, T. A.; Moore, A. L. Artificial Photosynthesis: From Molecular to Hybrid Nanoconstructs. In *From Molecules to Materials: Pathways to Artificial Photosynthesis*, Rozhkova, E. A.; Ariga, K., Eds. Springer International Publishing: Cham, 2015; pp 71-98.
5. House, R. L.; Iha, N. Y. M.; Coppo, R. L.; Alibabaei, L.; Sherman, B. D.; Kang, P.; Brennaman, M. K.; Hoertz, P. G.; Meyer, T. J. Artificial photosynthesis: Where are we now? Where can we go? *J. Photochem. Photobiol. C* **2015,** *25*, 32-45.
6. Fukuzumi, S.; Lee, Y.-M.; Nam, W. Bioinspired artificial photosynthesis systems. *Tetrahedron* **2020,** *76* (14), 131024.
7. Gaut, N. J.; Adamala, K. P. Toward artificial photosynthesis. *Science* **2020,** *368* (6491), 587.
8. Ye, S.; Ding, C.; Liu, M.; Wang, A.; Huang, Q.; Li, C. Water Oxidation Catalysts for Artificial Photosynthesis. *Adv. Mater.* **2019,** *31* (50), 1902069.
9. Zhang, B.; Sun, L. Artificial photosynthesis: opportunities and challenges of molecular catalysts. *Chem. Soc. Rev.* **2019,** *48* (7), 2216-2264.
10. Dogutan, D. K.; Nocera, D. G. Artificial Photosynthesis at Efficiencies Greatly Exceeding That of Natural Photosynthesis. *Acc. Chem. Res.* **2019,** *52* (11), 3143-3148.
11. Fujishima, A.; Honda, K. Electrochemical Photolysis of Water at a Semiconductor Electrode. *Nature* **1972,** *238* (5358), 37-38.
12. Grätzel, M. Photoelectrochemical cells. In *Materials for Sustainable Energy*, Co-Published with Macmillan Publishers Ltd, UK: 2010; pp 26-32.
13. Ohashi, K.; McCann, J.; Bockris, J. O. M. Stable photoelectrochemical cells for the splitting of water. *Nature* **1977,** *266* (5603), 610-611.
14. Barber, J. Photosystem II: the engine of life. *Q. Rev. Bio.* **2003,** *36* (1), 71-89.
15. Barber, J. Photosystem II: an enzyme of global significance. *Biochem. Soc. Trans.* **2006,** *34* (5), 619-631.
16. Vinyard, D. J.; Ananyev, G. M.; Charles Dismukes, G. Photosystem II: The Reaction Center of Oxygenic Photosynthesis. *Annu. Rev. Biochem* **2013,** *82* (1), 577-606.
17. Megiatto, J. D.; Antoniuk-Pablant, A.; Sherman, B. D.; Kodis, G.; Gervaldo, M.; Moore, T. A.; Moore, A. L.; Gust, D. Mimicking the electron transfer chain in photosystem II with a molecular triad thermodynamically capable of water oxidation. *Proc. Natl. Acad. Sci.* **2012,** *109* (39), 15578.

18. Moore, G. F.; Hambourger, M.; Kodis, G.; Michl, W.; Gust, D.; Moore, T. A.; Moore, A. L. Effects of Protonation State on a Tyrosine−Histidine Bioinspired Redox Mediator. *J. Phys. Chem. B* **2010,** *114* (45), 14450-14457.
19. Parr, R. G. In *Density Functional Theory of Atoms and Molecules*, Horizons of Quantum Chemistry, Dordrecht, 1980//; Fukui, K.; Pullman, B., Eds. Springer Netherlands: Dordrecht, 1980; pp 5-15.
20. Stratmann, R. E.; Scuseria, G. E.; Frisch, M. J. An efficient implementation of time-dependent density-functional theory for the calculation of excitation energies of large molecules. *J. Chem. Phys.* **1998,** *109* (19), 8218-8224.
21. Runge, E.; Gross, E. K. U. Density-Functional Theory for Time-Dependent Systems. *Phys. Rev. Lett.* **1984,** *52* (12), 997-1000.
22. Adamo, C.; Jacquemin, D. The calculations of excited-state properties with Time-Dependent Density Functional Theory. *Chem. Soc. Rev.* **2013,** *42* (3), 845-856.
23. Jacquemin, D.; Mennucci, B.; Adamo, C. Excited-state calculations with TD-DFT: from benchmarks to simulations in complex environments. *PCCP* **2011,** *13* (38), 16987-16998.
24. Jacquemin, D.; Perpète, E. A.; Assfeld, X.; Scalmani, G.; Frisch, M. J.; Adamo, C. The geometries, absorption and fluorescence wavelengths of solvated fluorescent coumarins: A CIS and TD-DFT comparative study. *Chem. Phys. Lett.* **2007,** *438* (4), 208-212.
25. Chiariello, M. G.; Rega, N. Exploring Nuclear Photorelaxation of Pyranine in Aqueous Solution: an Integrated Ab-Initio Molecular Dynamics and Time Resolved Vibrational Analysis Approach. *J. Phys. Chem. A* **2018,** *122* (11), 2884-2893.
26. Dreuw, A.; Head-Gordon, M. Failure of Time-Dependent Density Functional Theory for Long-Range Charge-Transfer Excited States: The Zincbacteriochlorin−Bacteriochlorin and Bacteriochlorophyll−Spheroidene Complexes. *JACS* **2004,** *126* (12), 4007-4016.
27. Tozer, D. J.; Amos, R. D.; Handy, N. C.; Roos, B. O.; Serrano-Andres, L. Does density functional theory contribute to the understanding of excited states of unsaturated organic compounds? *Mol. Phys.* **1999,** *97* (7), 859-868.
28. Noodleman, L.; Norman, J. G. The Xα valence bond theory of weak electronic coupling. Application to the low- lying states of Mo2Cl84−. *J. Chem. Phys.* **1979,** *70* (11), 4903-4906.
29. Noodleman, L. Valence bond description of antiferromagnetic coupling in transition metal dimers. *J. Chem. Phys.* **1981,** *74* (10), 5737-5743.
30. Norman, J. G.; Ryan, P. B.; Noodleman, L. Electronic structure of 2-Fe ferredoxin models by X.alpha. valence bond theory. *JACS* **1980,** *102* (12), 4279-4282.
31. Ovchinnikov, A. A.; Labanowski, J. K. Simple spin correction of unrestricted density-functional calculation. *Phys. Rev. A* **1996,** *53* (6), 3946-3952.
32. Ciofini, I.; Daul, C. A. DFT calculations of molecular magnetic properties of coordination compounds. *Coord. Chem. Rev.* **2003,** *238-239*, 187-209.
33. Mataga, N.; Shibata, Y.; Chosrowjan, H.; Yoshida, N.; Osuka, A. Internal Conversion and Vibronic Relaxation from Higher Excited Electronic State of Porphyrins: Femtosecond Fluorescence Dynamics Studies. *J. Phys. Chem. B* **2000,** *104* (17), 4001-4004.

Table of Content.